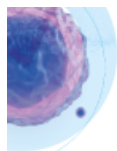


cPLA2 reversibly regulates different subsets of cancer stem cells transformation in cervical cancer

Yuchao He, Manyu Xiao, Hui Fu, Lu Chen, Lisha Qi, Dongming Liu, Piao Guo, Liwei Chen, Yi Luo, Huiting Xiao, Ning Zhang, Hua Guo



Introducing the CGX10 Cell Isolation System

The next-generation cell sorting system built for GMP-compliant cell and gene therapy manufacturing workflows



SONY

[Learn More](#)

cPLA2 α reversibly regulates different subsets of cancer stem cells transformation in cervical cancer

Yuchao He¹ | Manyu Xiao¹ | Hui Fu² | Lu Chen^{3,4} | Lisha Qi^{4,5} |
Dongming Liu^{4,5} | Piao Guo¹ | Liwei Chen¹ | Yi Luo¹ | Huiting Xiao⁶ |
Ning Zhang^{1,7} | Hua Guo¹ 

¹Department of Tumor Cell Biology, National Clinical Research Center for Cancer, Key Laboratory of Cancer Prevention and Therapy, Tianjin's Clinical Research Center for Cancer, Tianjin Medical University Cancer Institute and Hospital, Tianjin, People's Republic of China

²Tianjin University of Traditional Chinese Medicine, Tianjin, People's Republic of China

³Department of Hepatobiliary Tumor, Tianjin Medical University Cancer Institute and Hospital, Tianjin, People's Republic of China

⁴The Key Laboratory of Tianjin Cancer Prevention and Treatment, National Clinical Research Center for Cancer, Tianjin, People's Republic of China

⁵Department of Pathology, Tianjin Medical University Cancer Institute and Hospital, Tianjin, People's Republic of China

⁶Department of Gynecologic Oncology, Tianjin Medical University Cancer Institute and Hospital, Tianjin, People's Republic of China

⁷The Center for Translational Cancer Research, Peking University First Hospital, Beijing, People's Republic of China

Correspondence

Hua Guo, PhD, Tianjin Medical University Cancer Institute and Hospital, Tianjin 300060, People's Republic of China.

Email: guohua@tjmuch.com

Ning Zhang, PhD, Tianjin Medical University Cancer Institute and Hospital, Huan-hu-xi Road, He Xi District, Tianjin 300060, People's Republic of China.

Email: ningzhangtj@yahoo.com

Funding information

National Natural Science Foundation of China, Grant/Award Number: 31671421; Key Project of Tianjin Natural Science Foundation, Grant/Award Number: 18JCZDJC35200; NSFC-FRQS program, Grant/Award Number: 81661128009; State Key Project on Infectious Diseases of China, Grant/Award Number: 2018ZX10723204

Abstract

Cervical cancer stem cells (CCSCs) are considered major causes of chemoresistance/radioresistance and metastasis. Although several cell surface antigens have been identified in CCSCs, these markers vary among tumors because of CSC heterogeneity. However, whether these markers specifically distinguish CCSCs with different functions is unclear. Here, we demonstrated that CCSCs exist in two biologically distinct phenotypes characterized by different levels of cytosolic phospholipase A2 α (cPLA2 α) expression. Overexpression of cPLA2 α results in a CD44 $^+$ CD24 $^-$ phenotype associated with mesenchymal traits, including increased invasive and migration abilities, whereas CCSCs with cPLA2 α downregulation express CD133 and show quiescent epithelial characteristics. In addition, cPLA2 α regulates the reversible transition between mesenchymal and epithelial CCSC states through PKC ζ , an atypical protein kinase C, which governs cancer cell state changes and the maintenance of various embryonic stem cell characteristics, further inhibiting β -catenin-E-cadherin interaction in membrane and promoting β -catenin translocation into the nucleus to affect the transcriptional regulation of stemness signals. We propose that reversible transitions between mesenchymal and epithelial CCSC states regulated by cPLA2 α are necessary for cervical cancer metastasis and recurrence. Thus, cPLA2 α might be an attractive therapeutic target for eradicating different states of CCSCs to eliminate tumors more effectively.

KEY WORDS

cancer stem cells, CD133, CD24, CD44, cPLA2 α , epithelial-mesenchymal transition

Yuchao He, Manyu Xiao, and Hui Fu contributed equally to this work.

1 | INTRODUCTION

Cervical carcinoma (CC) is one of the most common types of gynecological malignancy worldwide and is the second leading cause of cancer death in young women aged 20 to 39 years, especially in developing countries.^{1,2} Despite the increases in screening programs and uptake of prophylactic human papillomavirus vaccination, the current standard treatments for CC—radiotherapy and chemotherapy—are less than satisfactory due to chemoresistance/radioresistance, lymph node metastasis, and pelvic recurrence.³

Cancer stem cells are the driving force or initiating factor of tumorigenesis and the seed of metastasis.⁴ However, a majority of cancer stem-like cells or tumor-initiating cells maintain a quiescent or dormant state and do not transform and metastasize until a change occurs in the microenvironment.^{5,6} The activation of epithelial-mesenchymal transition (EMT) program plays a key role in the acquisition of stem cell properties, the transformation of cancer stem cells (CSCs),^{7,8} and in tumorigenesis, invasion, metastasis, and drug resistance.⁹ In 2008, Weinberg et al first illustrated a direct link between EMT and CSCs, which was confirmed by multiple studies.⁷ Recently, Pastushenko et al showed that cancer cells undergoing EMT were subdivided into phenotypically and functionally distinct states.¹⁰ The plasticity between the different epithelial and mesenchymal states enables cancer cells to switch between the mesenchymal CSC state and the epithelial state, thereby creating intratumoral heterogeneity.¹¹ The CSC plasticity has been increasingly recognized as an important property of CSCs that drives therapeutic resistance and cancer relapse.¹²⁻¹⁶

CSCs exhibit plasticity that enables them to transition between different states with distinct phenotypes: EMT-like CSCs (with mesenchymal characteristics) and non-EMT-like CSCs (with epithelial characteristics).^{12,17} Furthermore, the EMT and non-EMT states of CSCs are not static but are instead plastic, allowing CSCs to transition between these two states.¹¹ Emerging evidence suggests that the transition between these phenotypes is regulated by the tumor microenvironment and may play a crucial role in the metastatic ability of these cells.^{12,13} Although both phenotypes have CSC features, such as high tumorigenicity, invasive nature, and resistance to chemotherapy and radiotherapy, whether these cells represent identical cancer cell populations and whether their characteristics are similar or distinct remain unclear. The mechanisms underlying the recurrence and metastasis associated with EMT and CSCs must be identified to design more suitable therapies for the different subpopulations of CSCs in various tissue-specific cancers.

Group IVA phospholipase A2 (cytosolic phospholipase A2 α [cPLA2 α]), the most extensively studied isoform in the cPLA2 family, is the only PLA2 isoform that shows specificity for phospholipid substrates containing arachidonic acid (AA).¹⁸ Metabolites produced by cPLA2 α , including AA, lysophosphatidic acid, thromboxane A₂, and prostaglandins, are implicated in the regulation of numerous cellular processes, including inflammation, mitogenesis, and tumorigenesis. For example, AA metabolism is associated with murine CSC apoptosis in leukemia.¹⁹ Our previous studies showed that cPLA2 α mediates

Significance statement

The study revealed for the first time that there are two morphologically and functionally distinct cancer stem cell populations regulated by cytosolic phospholipase A2 α (cPLA2 α) in cervical cancer. cPLA2 α might be a unique marker to identify different cancer stem cell populations and trigger quiescent epithelial cancer stem cell transformation to invasive mesenchymal states by regulating the phosphorylation of PKC ζ , which further inhibits β -catenin-E-cadherin interaction in membrane and promotes β -catenin translocation into the nucleus leading to metastasis and drug resistance. cPLA2 α , as a key to reversely regulating cervical cancer stem cell states and epithelial-mesenchymal transition, might provide innovative therapeutic strategies intended to halt tumor recurrence and metastasis.

tumor cell migration and invasion through TGF- β - and epidermal growth factor (EGF)-induced EMT in breast cancer and hepatocellular carcinoma.^{20,21} However, the functions of cPLA2 α in CSCs remain unknown, and the molecular mechanism requires further investigation.

In the present work, we investigated the regulatory function of cPLA2 α in different subsets of cervical cancer stem cells (CCSCs). Our results revealed that CCSCs exist in distinct epithelial-like and mesenchymal-like states characterized by cPLA2 α expression levels. The cells with high cPLA2 α expression are categorized in CD44 $^+$ CD24 $^-$ population with invasive mesenchymal traits, whereas those with low cPLA2 α expression are characterized as CD133 $^+$ with quiescent epithelial traits inversely regulated by the level of cPLA2 α . In addition, we elucidated the molecular mechanism underlying cPLA2 α regulation for the reversible transition between the epithelial-like and mesenchymal-like states in CCSCs. PKC ζ is targeted to further inhibit cell-to-cell adhesion, which is mediated by β -catenin-E-cadherin interaction and promotes β -catenin translocation into the nucleus to affect the transcriptional regulation of stemness signals. Based on the results of these studies, we propose that reversible transitions between epithelial-like and mesenchymal-like CCSCs regulated by cPLA2 α are necessary for CC metastasis and recurrence. Our findings may provide an attractive therapeutic approach, via targeting cPLA2 α , for future treatment strategies designed to target and more thoroughly eliminate different states of CCSCs.

2 | MATERIALS AND METHODS

2.1 | Patients and tissue specimens

A total of 99 patients with CC who underwent surgery at the Tianjin Medical University Cancer Institute and Hospital between December

2015 and January 2017 were included in this study. All paraffin-embedded specimens were examined by board-certified pathologists using hematoxylin and eosin (H&E) staining. Normal tissue that has been used as control in this study is a tumor-adjacent tissue, microscopically free from tumor depending on the pathological evaluation of HE staining. This study conformed to the ethical guidelines of the Declaration of Helsinki and was approved by the ethics committee.

2.2 | Cell culture

Human CC cell lines were purchased from the American Type Culture Collection (Manassas, Virginia). The cell lines were cultured in complete medium (DMEM for HeLa and SiHa cells) supplemented with 10% fetal bovine serum (FBS; PAN-Seratech) and 1% penicillin-streptomycin solution (HyClone) at 37°C in a humidified incubator with 5% CO₂.

2.3 | Immunohistochemistry

Cancer samples were infiltrated in xylene and a gradient concentration of ethanol, and antigen was then retrieved in citrate. Endogenous peroxidase activity was blocked with 3% H₂O₂ at room temperature for 10 minutes. Samples were stained using antibodies against cPLA₂ α (Santa Cruz Biotechnology, Santa Cruz, California), E-cadherin (BD Biosciences, New Jersey), or vimentin (Epitomics, California) at room temperature for 30 minutes and overnight at 4°C and were then washed with phosphate-buffered saline (PBS) and stained with secondary antibody for 1 hour at room temperature. The reaction product was developed using 3,3'-diaminobenzidine and counterstained with hematoxylin. Representative photomicrographs of immunostaining were acquired on a TissueFAXS (Tissue Gnostics). Staining was assessed in a blinded manner by two pathologists using a semiquantitative assay as follows.

The staining intensity of cPLA₂ α and E-cadherin was evaluated in three classes: 0, undetectable staining; 1, weak staining; and 2, strong staining. The percentage immunoreactivity score was classified on a 4-point scale: 0, < 10% positive cells; 1, 10%-40% positive cells; 2, 40%-70% positive cells; and 3, 70%-100% positive cells. Finally, the product of the staining intensity score and the percentage score was calculated as the final score, and the staining was graded as weak (−, a score of 0-3) or strong (+, a score of 4-6). Vimentin scoring was evaluated by a semiquantitative assay.²² The difference in the staining score between the nonmetastasis and metastasis groups was compared by a t test.

2.4 | Tumor sphere formation assay

For sphere cultures, cells were plated in ultra-low attachment 6-well plates (1000 cells per well) and cultured in serum-free DMEM/F12 medium supplemented with 2% B27, 20 ng/mL recombinant human

EGF, 20 ng/mL basic fibroblast growth factor, and 10 ng/mL recombinant human hepatocyte growth factor (all from Peprotech). Cells were cultured for more than 7 days in a humidified incubator maintained at 37°C with 5% CO₂.

2.5 | Single-cell sphere formation

cPLA₂ α KD or OE cells and control cells were plated into ultra-low attachment 96-well plates at a single-cell density using flow cytometric sorting and were incubated for 7 days. Spheres were digested into single-cell suspensions and counted. Then, the sphere proportions and the number of cells contained in a single sphere were microscopically determined.

2.6 | Sphere attachment and colony formation assays

Spheres were separated from the ultra-low attachment 6-well plates, reseeded into normal 10-cm dishes and allowed to attach. After the cells were attached, the cell colonies were quantified.

2.7 | Western blotting and antibodies

Cells were washed with cold PBS three times and lysed on ice for 30 minutes using SDS lysis buffer supplemented with 1 mM Naf, 1 mM Na₃VO₄, and 1× protease/phosphatase inhibitor cocktail (Roche, Switzerland). Nuclear and cytoplasmic proteins were extracted according to the instructions for the NE-PER nuclear and cytoplasmic extraction reagents (Thermo Scientific). The collected protein was denatured in a 95°C water bath for 10 minutes and centrifuged at 12 000 rpm at 4°C for 10 minutes. Equal amounts of protein were loaded on gels and separated by SDS-PAGE. Then, proteins were transferred to PVDF membranes (Immobilon-P; Millipore, Billerica, Massachusetts) and blocked with 5% milk or bovine serum albumin, followed by incubation with primary and secondary antibodies. The following antibodies were used: anti-cPLA₂ α from Gene Tex; anti-Histone from Proteintech; anti-GAPDH, anti-N-cadherin, anti-PKC ζ , goat anti-mouse IgG-HRP, and goat anti-rabbit IgG-HRP from Santa Cruz Biotechnology; anti-E-cadherin from BD Biosciences; anti-vimentin from Epitomics; anti-β-catenin from Abcam (Cambridge, UK); and anti-p-PKC ζ from Cell Signaling Technology (Beverly, Massachusetts). Details of the antibodies in the study are shown in Table S1.

2.8 | Transfection assay

The transfection assay was performed as described previously.²¹ Briefly, the packaging plasmids (VSVG and ΔR) and expression plasmids (KD, KD/SCR, OE, and OE/SCR) were transfected into HEK293T cells using Lipofectamine 2000 (Invitrogen) to produce lentiviral

particles. Then, cells were infected with the lentivirus to generate stable cPLA₂α KD or OE cells. In addition, the respective lentiviral vectors were transfected using the same methods, and the resulting cells were named KD/SCR and OE/SCR cells.

2.9 | RNA extraction, cDNA synthesis, and quantitative real-time PCR

Total RNA was isolated from adherent cells and spheres using TRIzol reagent (Ambion). cDNA was synthesized by RNA reverse transcription using a quantitative RT-PCR kit (Takara, Japan). The amplification reaction was performed according to the manufacturer's instructions (Takara, Japan) using predesigned primers. Primer sequences are listed in Table S2.

2.10 | Invasion assay

For the invasion assay, Matrigel-coated Transwell chambers were incubated in 24-well plates for more than 1 hour at 37°C. DMEM supplemented with 20% FBS was loaded in the lower chamber, and 2 × 10⁵ cells in serum-free DMEM were added to the upper chamber. After 24 hours incubation at 37°C in a humidified incubator with 5% CO₂, the invaded cells on the bottom were fixed with 4% paraformaldehyde for 20 minutes, stained, and counted by light microscopy.

2.11 | Chemotaxis assay

For the chemotaxis assay, DMEM supplemented with 10% FBS was loaded in the lower chamber, and 1 × 10⁵ cells in serum-free DMEM were seeded on the 8-μm polyvinyl pyrrolidone-free polycarbonate filter membrane. After incubation for 6 hours at 37°C in a humidified incubator containing 5% CO₂, the migrated cells on the bottom were fixed and stained and were counted by light microscopy.

2.12 | Scratch assay

For the scratch assay, cells were plated in 6-well plates at a density of 2 × 10⁶ cells/mL. After the cells were confluent and attached, a uniform wound was created using a 10-μL pipette tip. The cells were incubated for 24 hours at 37°C in a humidified incubator with 5% CO₂. The width of the wound was recorded at six random locations at the appropriate time points (0, 3, 6, 9, 12, and 24 hours). Data are shown as the means and standard deviations (SDs). Images were acquired at 0 and 24 hours.

2.13 | Colony formation assay

For the colony formation assay, 1000 cells in DMEM supplemented with 10% FBS were plated in 6-well plates. After 2 weeks of

incubation, the surviving colonies were fixed, stained with 0.5% crystal violet, imaged and counted, and the data are presented as the means ± SDs of triplicate dishes in the same experiment.

2.14 | Flow cytometric analysis of cell cycle distribution

Cells were digested, added to 95% ethanol and left at 4°C overnight. After centrifugation and washing, cells were stained with 500 μL of propidium iodide (PI; BD Biosciences) and incubated in the dark for 15 minutes. Samples were analyzed on a FACS Aria flow cytometer (BD) with CellQuest software, and the data were analyzed using FlowJo software.

2.15 | Flow cytometric analysis of cell apoptosis

The cell apoptosis assay was carried out according to the instructions of the FITC Annexin V Apoptosis Detection Kit (BD Pharmingen). Cells were digested and resuspended in 1× binding buffer. The solution was stained in 1.5-mL tubes with 5 μL of FITC annexin V and 5 μL of PI for 15 minutes at room temperature (25°C) in the dark. Finally, 400 μL of 1× binding buffer was added to each tube. Samples were analyzed on the FACS Aria flow cytometer with CellQuest software, and the data were analyzed with FlowJo software.

2.16 | Fluorescence-activated cell sorting and immunofluorescence

Determine the cell number and centrifuge the cell suspension at 300g for 10 minutes. Aspirate the supernatant completely and resuspend up to 10⁷ nucleated cells per 100 μL of PEB buffer. Add 10 μL of CD44, CD24 or CD133 antibody and the corresponding isotype antibody (Miltenyi Biotec). Then, mix well and incubate for 10 minutes in the dark in the refrigerator (2–8°C). Wash the cells by adding 1–2 mL of buffer and centrifuge at 300g for 10 minutes. Aspirate the supernatant completely and resuspend the cell pellet in a suitable amount of buffer for analysis by flow cytometry (BD). The sorted CD44⁺CD24[−] and CD133⁺ cells were lysed and amplified by the Smart-Seq method to obtain cDNA for RT-PCR analysis. Immunofluorescence was performed as described previously.²¹

2.17 | Cell viability assay

Cells were plated in a 96-well plate at 5000 cells/well and treated with cisplatin at the indicated gradient concentrations for 48 hours. Then, 10 μL of CCK-8 reagent (Dojindo) was added and coincubated with the cells for 4 hours. The absorbance was measured, including the detection wavelength at 450 nm and the reference wavelength at

650 nm. Cell viability was calculated using the following formula: Cell viability = [(As – Ab)/(Ac – Ab)] × 100% (where As is the absorbance of the experimental well; Ab is the absorbance of the blank well; and Ac is the absorbance of the control well).

2.18 | Co-immunoprecipitation, silver staining, and liquid chromatography-tandem mass spectrometry

The purified proteins from HeLa cells were lysed with Triton X-100 lysis buffer containing protease inhibitor cocktail (Roche). Rabbit anti-cPLA₂ α antibody was incubated with protein A beads (Invitrogen) at 4°C for 6 hours. Then cPLA₂ α and its interacting proteins were purified with the antibody conjugated beads overnight, followed by Western blotting and silver staining with a silver staining kit following the manufacturer's protocol (Pierce). Each distinct gel band was retrieved, digested, and analyzed by liquid chromatography-tandem mass spectrometry using Orbitrap Fusion Lumos Tribrid mass spectrometer.

2.19 | Microarray analysis

The microarray gene expression analysis of cPLA₂ α KD spheres and KD/SCR spheres was performed using GeneChip Clariom S Array (Human, Affymetrix) and further analyzed by Ingenuity Pathway Analyses (Ingenuity Systems, California).

2.20 | Mouse xenograft tumor model

For the animal experiments, 4- to 8-week-old NOD-SCID nude mice were purchased from the Model Animal Research Center of Nanjing University. Additionally, different numbers of cPLA₂ α KD or OE cells and control cells were subcutaneously injected into the armpit of the mice as indicated (n = 5 per group). After injection, the mice were monitored, and the tumor sizes were measured daily using a caliper. The mice were sacrificed at 38 days post-inoculation. The tumor volumes were calculated by the following formula: V (mm³) = L × W × W × 0.5 (where L is the length and W is the width of the tumor). The tumor growth rate was specifically recorded at distinct time points. All the mouse experiments were carried out according to the guidelines approved by the Committee on the Ethics of Animal Experiments of Tianjin Medical University Cancer Institute and Hospital.

2.21 | Gene set enrichment analysis

Gene set enrichment analysis (GSEA) was performed to determine whether the cPLA₂ α mRNA level is related to biological states, including metastasis and EMT, on the basis of GSEA-9750 data sets for CC using GSEA 2.0.9 (<http://software.broadinstitute.org/gsea/index.jsp>).

2.22 | Statistical analyses

All data are shown as the means ± SDs. Differences between groups were evaluated by a two-tailed Student's *t* test or ANOVA. Statistical significance was defined as *P* < .05. For data from human samples, the 1-year recurrence-free survival (RFS) was measured from the date of operation to the last day of follow-up. The two groups were compared using Student's *t* test for parametric data and a Mann-Whitney *U* test for nonparametric data. RFS curves were generated using the Kaplan-Meier method and compared using the log-rank test. The prognostic factors were determined by Cox regression analysis. All statistical analyses were performed using SPSS Version 21.0 for Windows (SPSS Inc., Chicago, Illinois).

3 | RESULTS

3.1 | cPLA₂ α identifies distinct CC stem-like cells with distinct epithelial and mesenchymal biomarker expression profiles

Spheroid culture in stem cell-selective conditions is a routine approach to enrich CSCs, and the sphere formation ability is considered indicative of the fundamental properties of CSCs, such as self-renewal, potent pluripotency, and tumorigenesis.^{3,23} We first observed an interesting phenomenon in HeLa cells with stable cPLA₂ α overexpression (OE) and cPLA₂ α downregulation (KD) via transfection with different lentiviral plasmids (Figure 1A). cPLA₂ α KD cells presented epithelial-type tight spheres in serum-free medium, an *in vitro* model of CSCs, whereas cPLA₂ α OE cells formed mesenchymal-type loose grape-shaped clusters (Figure 1B). Flow cytometric analysis of a CC stemness marker (ABC transporter ABCG2) and RT-PCR analysis of pluripotency transcription factors (NANOG, OCT4, and SOX2) demonstrated that the enriched spheres had higher expression levels of ABCG2, NANOG, SOX2 than their corresponding adherent cells, indicating that the enriched spheres had stem cell characteristics (Figure 1C,D). RT-PCR analysis further demonstrated that cPLA₂ α KD spheres were enriched for the expression of epithelial genes (Figure 1E). As assessed by immunofluorescence and Western blot analysis, the cPLA₂ α KD spheres displayed epithelial morphology characterized by the expression of mesenchymal–epithelial transition (MET) marker E-cadherin and the inhibition of EMT marker vimentin (Figure 1F,G). In contrast, cPLA₂ α OE spheres exhibited a reciprocal mesenchymal gene expression pattern (Figure 1H,I), suggesting that CCSCs with different cPLA₂ α levels represented distinct populations of CCSCs with distinct epithelial and mesenchymal biomarker expression profiles.

To determine whether this process is cell-specific, we altered the expression of cPLA₂ α in other CC cell lines, namely C33A, HCC94, and SiHa. The mesenchymal markers and associated transcription factors were enriched in all cPLA₂ α OE groups (Figure S1D-F). The silencing of cPLA₂ α also increased the E-cadherin, OVOL1, and

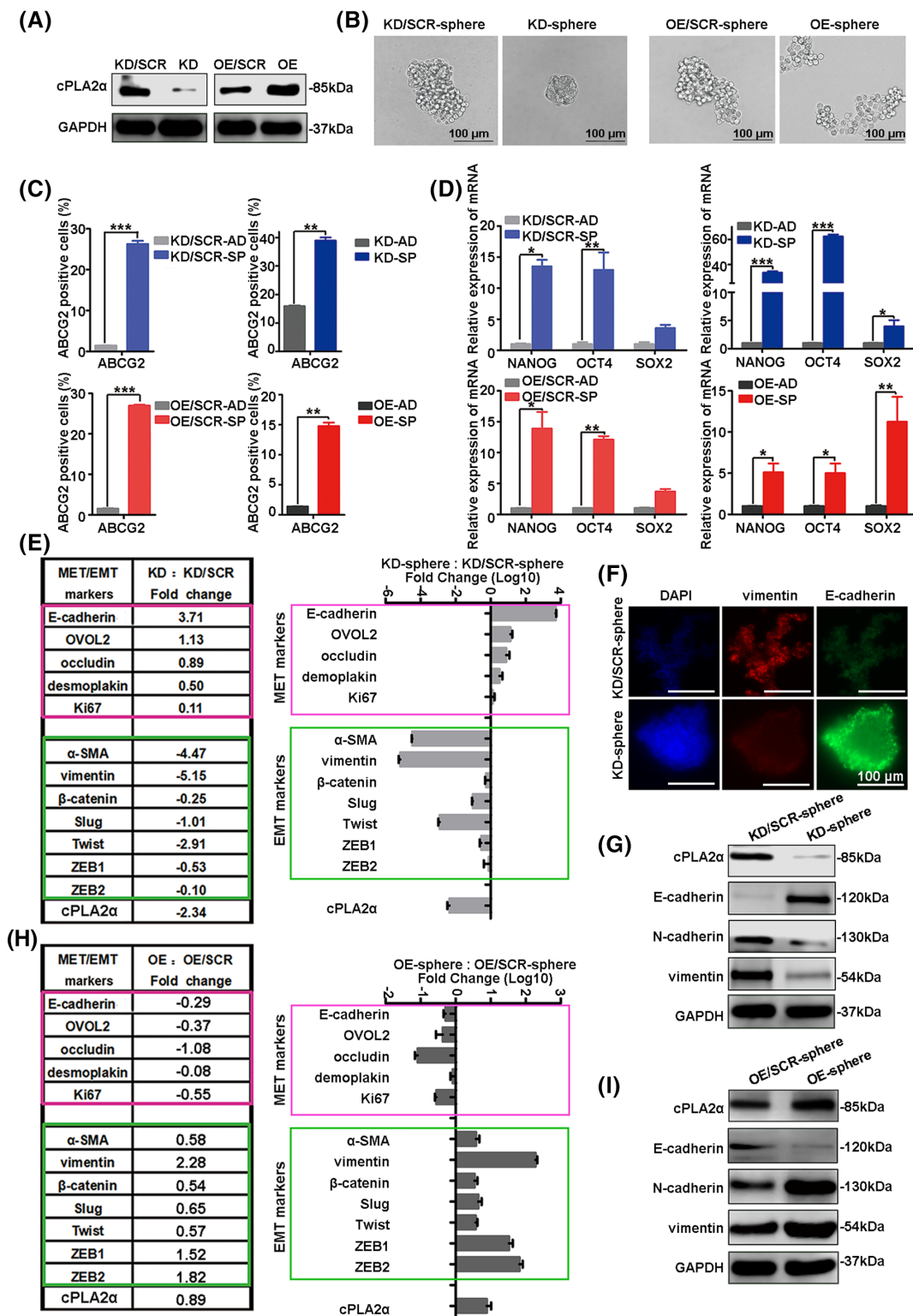


FIGURE 1 cPLA α identifies distinct cervical cancer stem-like cells with distinct EMT and MET marker expression profiles. A, Western blot verification of the transfection efficiency for the cPLA α KD and OE vectors in HeLa cells. B, cPLA α KD or OE spheres presented two distinct subpopulations with tight and loose shapes. Scale bars = 100 μ m. C, Flow cytometric analysis of cervical cancer stemness marker expression, ABCG2, enriched in spheres more than adherent cells. D, RT-PCR analysis of pluripotency transcription factors (NANOG, OCT4, SOX2) enriched in spheres more than adherent cells. E, Epithelial gene expression-enriched and EMT-associated genes decreased in the cPLA α KD spheres by RT-PCR assay. F, Staining of vimentin (red), E-cadherin (green), and DAPI (blue) in cPLA α KD spheres compared with KD/SCR spheres as assessed by immunofluorescence assay. Scale bars = 100 μ m. G, Western blotting revealed that cPLA α KD increased E-cadherin and decreased N-cadherin and vimentin expression at the protein level. H, Mesenchymal gene expression-enriched and MET-associated genes decreased in the cPLA α OE spheres. I, Western blotting revealed that cPLA α OE decreased E-cadherin and increased N-cadherin and vimentin expression at the protein level. (*P < .05; **P < .01; ***P < .001). cPLA α , cytosolic phospholipase A2 α ; EMT, epithelial-mesenchymal transition; MET, mesenchymal-epithelial transition

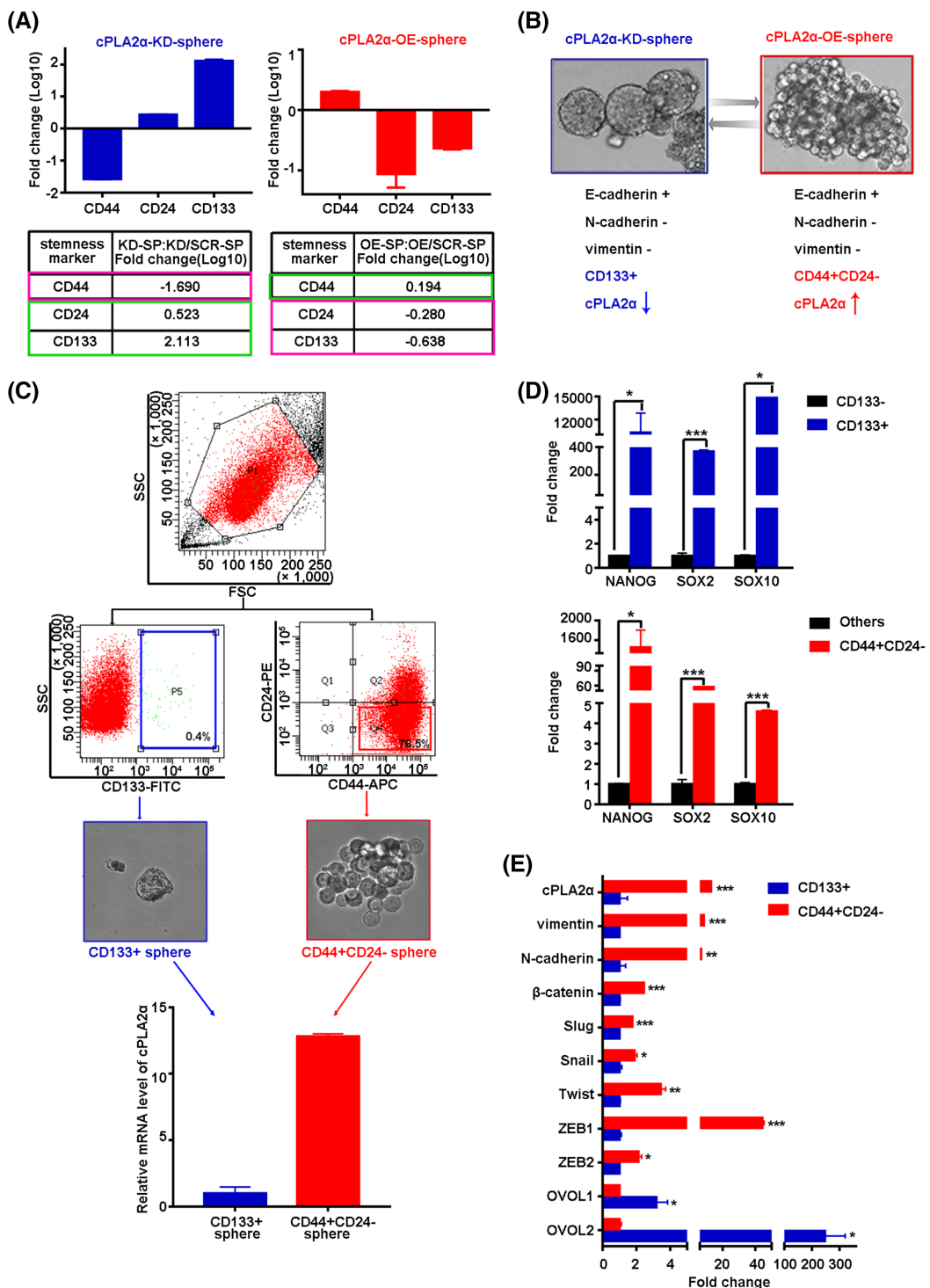


FIGURE 2 cPLA₂ α^{high} identifies CD44 $^{+}$ CD24 $^{-}$ mesenchymal CCSCs, and cPLA₂ α^{low} identifies CD133 $^{+}$ epithelial CCSCs. A, cPLA₂ α KD and OE spheres showed opposing CD44, CD24, and CD133 expression patterns by an RT-PCR assay. B, The model suggests that different expression levels of cPLA₂ α differentiate the CD44 $^{+}$ CD24 $^{-}$ CCSC phenotype with mesenchymal traits from the CD133 $^{+}$ CCSC phenotype with epithelial characteristics. C, HeLa cells were sorted into a CD44 $^{+}$ CD24 $^{-}$ population enriched for high cPLA₂ α expression and forming loose grape-shaped clusters and a CD133 $^{+}$ population with lower cPLA₂ α levels as detected by RT-PCR and forming the tight sphere. D, RT-PCR measurement of the levels of pluripotency transcription factors, including NANOG, SOX2, and SOX10, in the CD44 $^{+}$ CD24 $^{-}$ and CD133 $^{+}$ populations. E, EMT-associated genes, including vimentin, N-cadherin, β-catenin, Slug, Snail, Twist, ZEB1 and ZEB2, were enriched in the CD44 $^{+}$ CD24 $^{-}$ population, whereas the MET-related transcription factors OVOL1 and OVOL2 were correspondingly increased in the CD133 $^{+}$ population (* $P < .05$; ** $P < .01$; *** $P < .001$). CCSCs, cervical cancer stem cells; cPLA₂ α , cytosolic phospholipase A2 α ; EMT, epithelial-mesenchymal transition; MET, mesenchymal-epithelial transition

OVOL2 level in SiHa, C33A, and HCC94 cells, whereas cPLA α OE reversed the results (Figure S1A-C).

3.2 | cPLA α ^{high} identifies CD44⁺CD24⁻ mesenchymal CCSCs, and cPLA α ^{low} identifies CD133⁺ epithelial CCSCs

To further verify whether cPLA α can differentiate stem cell subtypes with different stemness markers, we performed serial stemness markers expression analysis via RT-PCR in cPLA α KD and OE spheres (data not shown). Interestingly, the two groups showed opposing expression patterns for CD44, CD24, and CD133 (Figure 2A). We evaluated the characteristics of CD44⁺CD24⁻ and CD133⁺ in three representative CC cell lines. CD44⁺CD24⁻ cells were detected in sorted SiHa, HCC94, and HeLa cells at the mean of 6.55%, 24.45%, and 81.25%, respectively. A small CD133⁺ cell population was observed and cPLA α ⁺ cells presented an increased trend (mean of 0.715% [SiHa], 6.69% [HCC94], and 23.1% [HeLa]) similar to CD44⁺CD24⁻ cells (Figure S2A,B). Moreover, cells with a high proportion of CD44⁺CD24⁻ also have high levels of vimentin and relatively low levels of E-cadherin (Figure S2C), suggesting that high cPLA α expression results in a CD44⁺CD24⁻ subset with a mesenchymal gene expression pattern, whereas low expression of cPLA α results in CD133⁺ CCSCs with epithelial characteristics (Figure 2B). Flow cytometry using CD44, CD24, and CD133 as markers in HeLa cells further verified that CD44⁺CD24⁻ cells were enriched for high expression of cPLA α and formed loose grape-shaped clusters, whereas CD133⁺ cells showed significantly lower cPLA α levels than CD44⁺CD24⁻ cells and formed tight spheres consistent with the morphology of the cPLA α KD group (Figure 2C). The stemness characteristics of these enriched spheres were also verified with increased levels of pluripotency transcription factors (NANOG, SOX2, and SOX10) (Figure 2D). In addition, mesenchymal-associated genes, including vimentin, N-cadherin, β -catenin, Slug, Snail, Twist, ZEB1, and ZEB2, were enriched in the CD44⁺CD24⁻ populations, whereas the level of the epithelial-related transcription factors OVOL1 and OVOL2²⁴ was correspondingly increased in the CD133⁺ populations (Figure 2E). Other mesenchymal markers (such as TGF- β , STAT3, and c/eBP β) and epithelial marker E-cadherin did not show significant difference (Figure S2D).

3.3 | cPLA α promotes the transformation of quiescent stem-like cells to malignant status

To explore the functional difference in the two stem cell subsets, we utilized GeneChip Clariom S Array (Human, Affymetrix) to evaluate the differential expression genes between cPLA α KD spheres and KD/SCR spheres. Scatter plot (Figure S3A) showed the distribution of the signal intensity in the Cartesian coordinate system. The parallel green lines were the differential reference lines, the red points outside the interval of the reference line represented the probes relatively upregulated in the KD group ($n = 1314$), and the green points represented the probes

relatively downregulated in the KD spheres compared with those in the KD/SCR spheres ($n = 1470$). Volcano plot (Figure S3B) showed the distribution of the differentially expressed genes between the KD and KD/SCR groups. The red points represented the significantly different genes screened by |Fold change| ≥ 2.0 and FDR < 0.05 . Analysis of disease and function revealed that the significant enrichment of differential genes was closely related to cancer, cellular movement, cell death and survival, cellular growth, and proliferation (Figure S3C). The tumor cell line proliferation, colony formation, cell cycle progression, tumor cell line movement, migration, and invasion were suppressed, whereas tumor cell line adhesions were activated (Figure 3A).

To verify the stem cell function of different populations regulated by cPLA α , we seeded single cells in ultra-low attachment 96-well plates by flow cytometric sorting to form single spheres after 1 week (Figure 3B) and observed that cPLA α OE spheres were larger and contained more cells than the OE/SCR spheres, indicating the augmented proliferation in the cPLA α overexpression group. The 96-well plate sphere formation assay illustrated that cPLA α OE dramatically increased and cPLA α KD blocked the cancer stem-like cell sphere formation ability (Figure 3B). Consistently, G0/G1 phase was arrested when cPLA α expression was reduced (from $61.08\% \pm 1.07\%$ to $67.23\% \pm 2.34\%$), whereas cPLA α OE cells entered the cell cycle with a decreased percentage of G0/G1-phase cells, accompanied by S + G2/M phase extension (from $41.67\% \pm 4.45\%$ to $57.09\% \pm 2.28\%$) (Figure 3C). A similar phenomenon was observed in SiHa cells, in which cPLA α KD induced a low level of cell cycle arrest in the G0/G1 phase (Figure S4E). In addition, the higher apoptosis rate in the KD sphere group may also further reduce proliferation and tumor formation (Figure S4B). Further analysis of tumorigenesis *in vivo* verified that cPLA α OE spheres displayed an increased tumor initiation capacity in NOD-SCID mice compared with that of OE/SCR spheres (1000 cells injected), OE adherent cells (10 000 cells injected), and, on the 19th day after injection, OE spheres (1000 cells injected) (Figure 3D). However, neither the adherent cells nor the spheres in the KD group from HeLa cell line and KD spheres from SiHa cell line (3000 cells injected) were tumorigenic, showing a relatively quiescent status (Figure S4G).

Except proliferation, tumor cells migration, invasion, and movement were inhibited in cPLA α KD spheres (Figure 3A) and GSEA evaluation further revealed the correlation of cPLA α mRNA expression with cell migration, invasiveness, and metastasis (Figure 4A). Simultaneously, cPLA α increased the invasion ability of cancer stem-like cells in HeLa (Figure 4B). Transwell assays and wound assays showed that cPLA α upregulation markedly increased the cell migration ability, whereas KD of cPLA α induced an apparent decrease in SiHa cells (Figure S4C,D). Ten spheres from OE, OE/SCR, KD, and KD/SCR cells were isolated by pipetting and plated into normal dishes to determine their ability to reattach to substrates. The spheres were examined for 10 days; cPLA α OE spheres were substantially more competent at adhering to substrates and spread faster and wider out of the spheroid bodies than OE/SCR spheres. However, the quantification results indicated that KD spheres had difficulty reattaching and spreading. The final colony formation staining results further confirmed this pattern (Figure 4C and Figure S4A). This phenomenon may be due to cell cycle arrest and

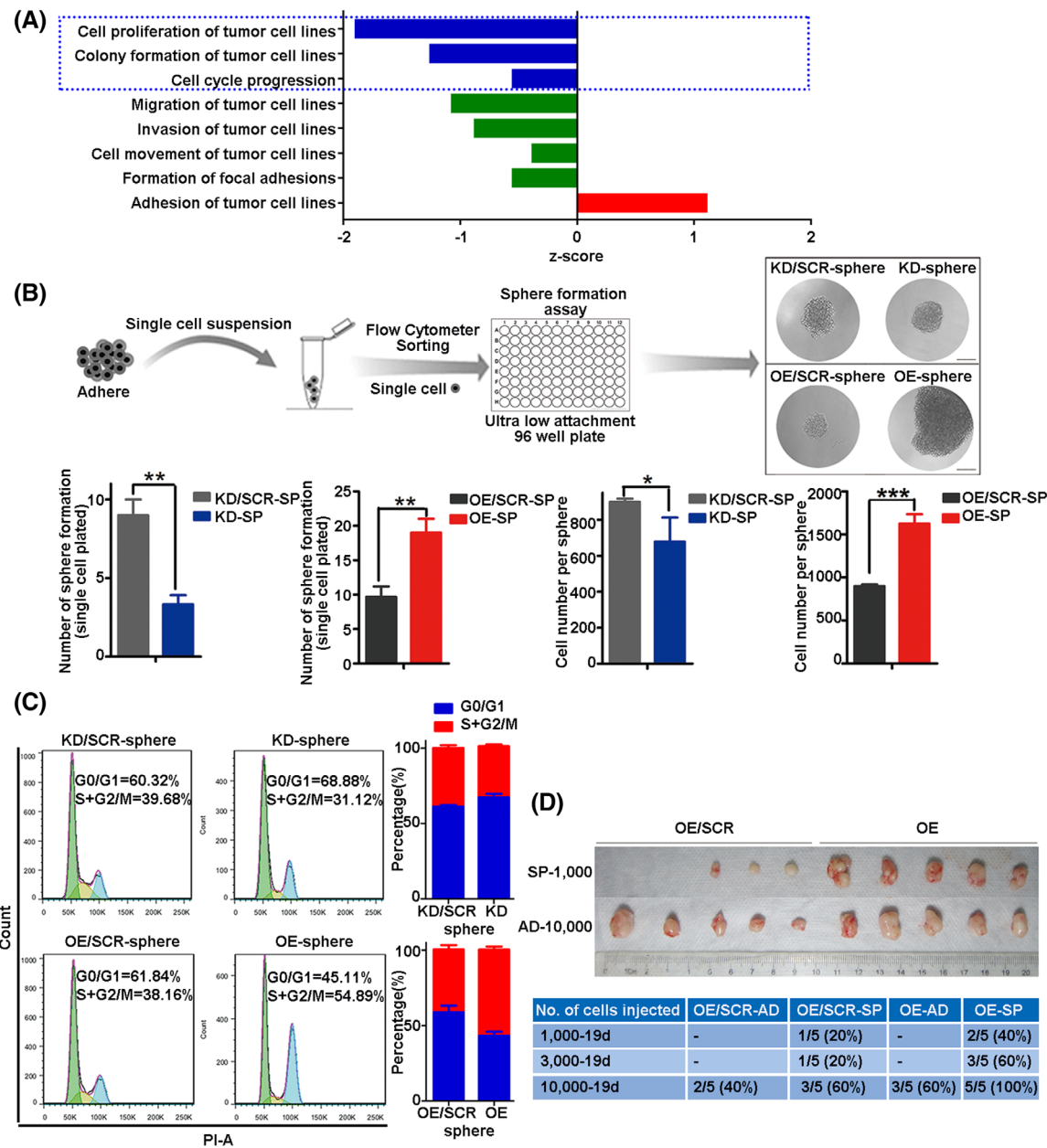


FIGURE 3 cPLA₂ α promotes the transformation of quiescent stem-like cells to malignant status, which display high proliferation and tumorigenic ability. A, The relationship between the level of differential genes and activation and inhibition of disease and function. Red indicates that the disease or functional state is activated (Z-score > 0), blue and green means that the disease or functional state is suppressed (Z-score < 0). Suppressed functions include tumor cell lines proliferation (-1.891), colony formation (-1.629), tumor cell lines movement (-0.378), migration (-1.069), invasion (-0.873), and formation of focal adhesions (-0.548). Activated functions include adhesion of tumor cell lines (1.105). B, Flow cytometric sorting to form single spheres and comparison of sphere formation rates. Scale bars = 50 μ m. C, The cell cycle distribution of the spheres showed that cPLA₂ α KD induced cell cycle arrest in G0/G1 phase. In contrast, cPLA₂ α OE decreased the percentage of G0/G1-phase cells, accompanied by S + G2/M phase extension. D, Different numbers of cPLA₂ α KD or OE adherent and spheroid cells and control cells were subcutaneously injected into mice as indicated (n = 5 per group). cPLA₂ α OE spheres exhibited an increased tumor initiation capacity (*P < .05; **P < .01; ***P < .001). cPLA₂ α , cytosolic phospholipase A2 α .

adhesion signal regulation. Cell-to-cell adhesion signals were enriched, and the focal adhesion to the extracellular matrix (ECM) signals was weakened in the KD spheres (Figure 4D). Cell adhesion assay further revealed that the attachment cell numbers of cPLA₂ α KD spheres to fibronectin at 5 and 15 minutes were significantly reduced. Conversely, cPLA₂ α OE spheres increased the attachment ability to ECM compared with that of control spheres in SiHa (Figure S4F). This phenomenon led

to difficult adhesion and passage through the matrix, resulting in EMT and cancer metastasis. Similar results were demonstrated in adherent HeLa cells in which the cPLA₂ α expression enhanced cell migration, invasion, proliferation, colony formation ability, and EMT (Figures S5A-G). These results were consistent with the cell cycle status of CD133 $^+$ CSCs which showed an increased proportion of cells in the G0-G1 phase and maintained a quiescent state,²⁵ whereas overexpression of the

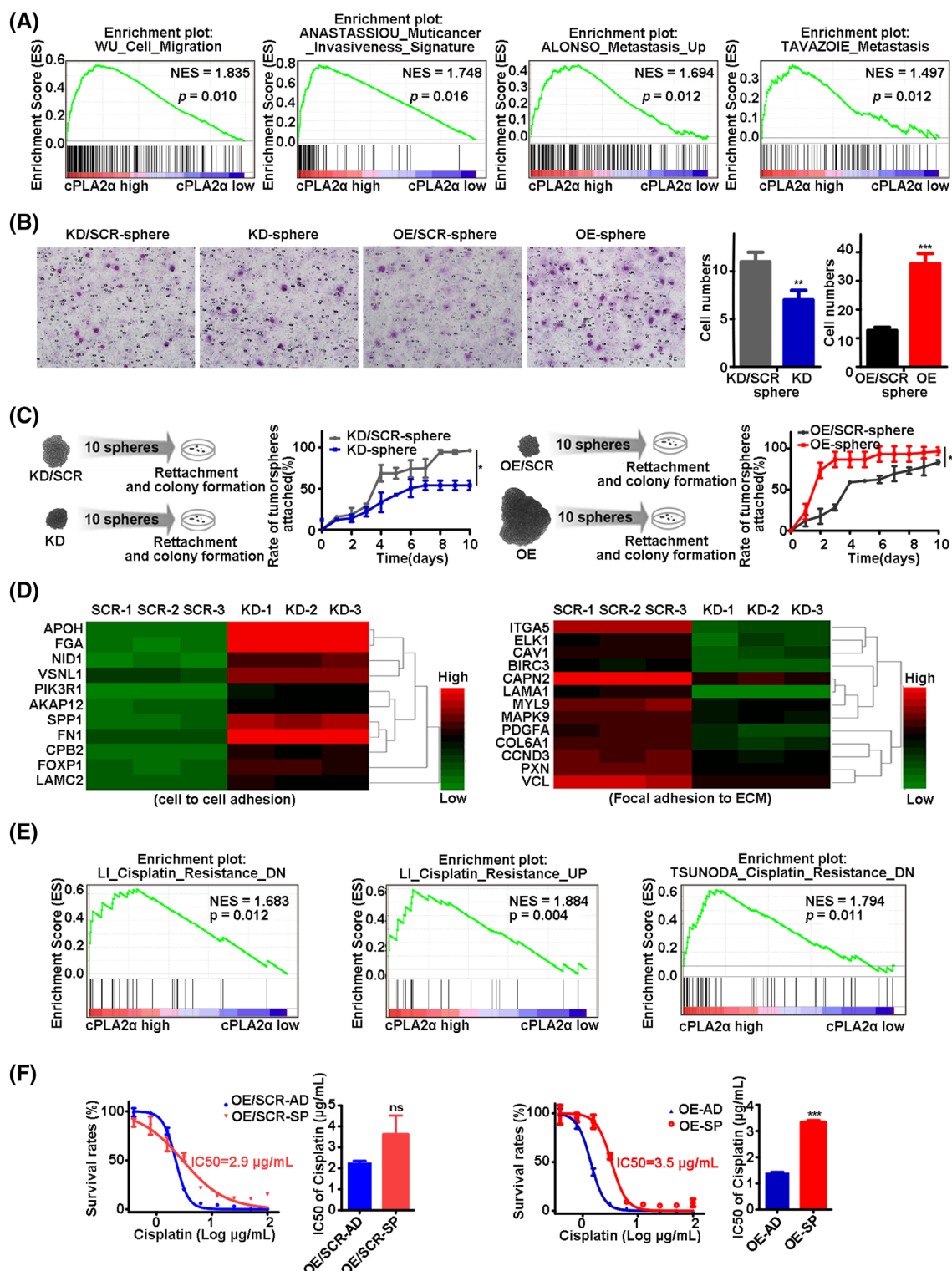


FIGURE 4 cPLA α promotes the transformation of quiescent stem-like cells to malignant status, which display high invasion, and adhesion abilities; spreading characteristics; and drug resistance. **A**, GSEA was performed to evaluate the correlation of cPLA α mRNA expression with cell migration, invasiveness, and metastasis on the basis of GSEA-9750 data sets. **B**, An invasion assay with the spheres showed that cPLA α accelerated the invasion of cancer stem-like cells. **C**, Ten spheres of OE, OE/SCR, KD, and KD/SCR cells were isolated by pipetting and plated into normal dishes to determine the substrate reattachment ability and spreading capacity. **D**, Heat map showed enriched different genes associated cell-cell adhesion and focal adhesion to ECM between KD/SCR and KD spheres by microarray analysis. Red and green depict high and low expression levels, respectively, as indicated by the scale bar. **E**, Correlation between cPLA α and cisplatin resistance from the analysis of GSEA-9750 data sets. **F**, IC50 analysis of cisplatin sensitivity by a CCK-8 assay in OE/SCR and OE adherent or spheroid cells. (*, P < .05; **, P < .01; ***, P < .001). cPLA α , cytosolic phospholipase A2 α ; ECM, extracellular matrix; GSEA, gene set enrichment analysis.

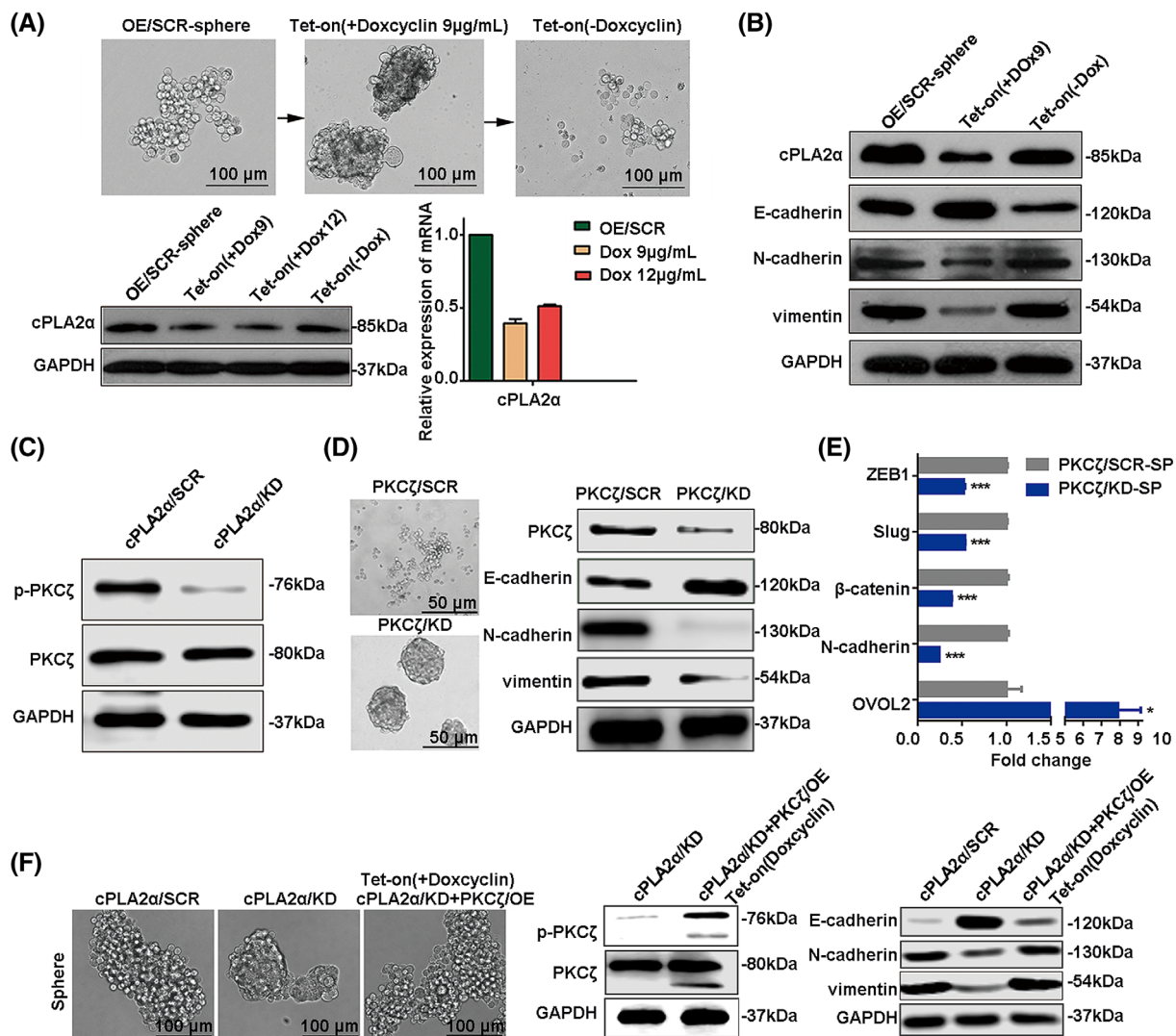


FIGURE 5 cPLA α reversibly regulates the transformation of distinct CCSCs subsets through PKC ζ . **A** and **B**, In a Tet-on inducible system initiated with 9 or 12 μ g/mL doxycycline, cPLA α expression decreased, and cells formed tight spheres with high expression of E-cadherin (**B**), whereas the removal of doxycycline rescued the sphere shape and EMT-related gene expression. Scale bars = 100 μ m. **C**, PKC ζ phosphorylation levels were reduced in cPLA α KD cells, as determined by Western blotting. Scale bars = 50 μ m. **D**, PKC ζ shRNA was transfected into HeLa cells to generate PKC ζ KD cells, which formed a tight sphere shape. Cellular protein extracts and total RNA were prepared and analyzed by Western blotting and RT-PCR (**E**) to determine the expression levels of EMT/MET-related genes. **F**, The PKC ζ overexpression cell line was established using the Tet-on inducible system on the basis of cPLA α KD cells and cultured in serum-free medium to enrich for spheres. The extracted protein from cPLA α SCR, cPLA α KD, and PKC ζ OE cells was analyzed by Western blotting to determine the levels of PKC ζ and EMT-associated genes. Scale bars = 100 μ m (*, P < .05; ***, P < .001). CCSCs, cervical cancer stem cells; cPLA α , cytosolic phospholipase A2 α ; EMT, epithelial-mesenchymal transition; MET, mesenchymal-epithelial transition

CD44v6 protein closely correlates with the tumorigenesis, metastasis, and prognosis of uterine CC.²⁶ Notably, the GSEA results from multiple data sets showed that high expression of cPLA α was positively associated with cisplatin resistance (Figure 4E). Furthermore, cPLA α OE stem-like cells exhibited stronger chemoresistance with a higher IC50 of cisplatin than progenitor adherent cells ($3.61 \pm 0.91 \mu$ M vs $1.42 \pm 0.02 \mu$ M), whereas the difference between OE/SCR spheres and OE/SCR adherent cells was not significant (Figure 4F).

These results suggest that the epithelial CCSCs with low cPLA α expression are relatively quiescent, and cPLA α may trigger the transformation of quiescent stem-like cells to exhibit a progressive status

and increased proliferation, invasion, adhesion and spreading ability, and drug resistance and facilitate tumor initiation and development.

3.4 | cPLA α reversibly regulates the transformation of distinct CCSCs subsets through PKC ζ

To verify whether cPLA α truly mediates the transition between the quiescent epithelial-like and invasive mesenchymal-like stem cell states, we used a Tet-on inducible system and determined the sphere

phenotype and EMT-related gene expression levels. The Tet-on inducible system can efficiently generate stable human Tet-on cell lines that reliably drive either inducible overexpression or knockdown of the gene of interest.²⁷ When the Tet-on system was induced with 9 or 12 µg/mL doxycycline, cPLA₂α expression decreased, and the cells formed tight spheres with high expression of E-cadherin. However, when doxycycline was removed, the sphere state changed from a tight form to a loose pattern, and high expression levels of N-cadherin and vimentin were rescued (Figure 5A-B).

To study the regulatory mechanism in the distinct CCSC populations, we investigated 452 key proteins with 582 phosphorylation sites covering canonical pathways between the cPLA₂α OE and KD groups using a Phospho Explorer Antibody microarray (PEX100). KEGG pathway analysis revealed that proteins with significantly altered expression were mainly enriched in the PI3K/Akt and MAPK signaling pathways (Figure S6A). This finding was consistent with the report that the PI3K pathway is associated with stem cell maintenance as well as EMT.^{28,29} Moreover, consistent with this observation, we identified PKCζ, a calcium- and diacylglycerol-independent serine/threonine-protein kinase that functions in the PI3K pathway and MAPK cascade and is involved in cell proliferation, cell survival, EMT, and stemness,³⁰⁻³² and its phosphorylation level was reduced in cPLA₂α KD cells (Figure 5C). To determine whether cPLA₂α regulates stem cell states through PKCζ, PKCζ shRNA was transfected into HeLa cells to generate PKCζ KD cells, which formed a tight sphere shape (Figure 5D). In addition, downregulation of PKCζ increased E-cadherin expression but reduced N-cadherin and vimentin expression (Figure 5D). The increase in the levels of additional EMT-related markers (β-catenin) or transcription factors, including Slug and ZEB1, and the decline in OVOL2 expression further confirmed the above results (Figure 5E).

To further verify that cPLA₂α regulated stem states through PKCζ, we cultured PKCζ-overexpressing cells utilizing the Tet-on inducible system on the basis of cPLA₂α KD cells. The results showed that PKCζ overexpression rescued the sphere pattern to a loose shape with mesenchymal traits comparable to those of cPLA₂α KD cells (Figure 5F).

3.5 | cPLA₂α regulates phosphorylation of PKCζ, which further promotes β-catenin translocation into the nucleus to affect the stem cell phenotype

PKCζ has been reported to affect β-catenin stability, further affecting stem cell function.³³ Consistently, KEGG pathway analysis revealed that the differential genes between cPLA₂α KD and KD/SCR CSCs were enriched in Wnt/β-catenin pathway (Figure S7A). Close examination of the genes in the Wnt/β-catenin pathway was conducted using the heat map (Figure S7B) and verified by RT-PCR (Figure S7C). Mass spectrometry was performed to investigate cPLA₂α interactome. The results indicated that cPLA₂α was associated with multiple proteins including β-catenin (Figure 6A). Co-immunoprecipitation experiments were conducted using HeLa cell extracts to confirm the association of cPLA₂α with β-catenin, and the results verified the interaction (Figure 6B).

As a key regulator in the Wnt pathway and in the formation of adherent junction, most of the β-catenin molecules are distributed in the cell membrane, form a complex with E-cadherin, and mediate cell-to-cell adhesion; the remaining β-catenin is dissociated in the cytoplasm and degraded by protease under physiological conditions.³⁴ We found that more β-catenin was bound to the cytomembrane with E-cadherin when cPLA₂α was knocked down, with increased E-cadherin-mediated cell-cell adhesion (Figure 6C). In addition, β-catenin degradation was slowed down (Figure 6D) when PKCζ was knocked down and treated with protein synthesis inhibitor cycloheximide (CHX); however, nuclear translocation of β-catenin was reduced as shown by the Western blot analysis (Figure 6E) and immunofluorescence localization assay (Figure 6F). The loss of nuclear β-catenin was rescued when PKCζ was reexpressed by adding doxycycline (Figure 6G). To further determine the role of β-catenin in contributing to EMT, shRNA-mediated silencing of β-catenin was performed and validated by Western blotting and RT-PCR. β-Catenin silencing caused a decrease in the levels of mesenchymal-associated genes, including vimentin, N-cadherin, α-SMA, and the transcription factors Slug, Twist, and ZEB1 (Figure 6H,I). Such results are consistent with a report that β-catenin is activated by E-cadherin loss and is necessary for E-cadherin-induced EMT.³⁵

3.6 | Elevated cPLA₂α expression is associated with CC metastasis and poor survival

In support of our deduction, we observed these two CCSC populations with epithelial and mesenchymal traits in CC tissues. As assessed by immunofluorescence utilizing antibodies against CD44, CD24, cPLA₂α, CD44⁺CD24⁻ and cPLA₂α⁺ identified overlapping stem cell populations in CC tissues near the edge (Figure 7A). In addition, the CD133⁺ population sorted from cervical tissues exhibited relatively low level of cPLA₂α and increased levels of epithelial genes, including E-cadherin, OVOL2, and desmoplakin, and decreased β-catenin level. Conversely, the levels of cPLA₂α and mesenchymal genes (vimentin and ZEB1) were increased in the CD44⁺CD24⁻ population, whereas the levels of E-cadherin and occludin, the markers associated with MET, showed a decreasing trend (Figure 7B,C). This was consistent with the results that cPLA₂α level was positively associated with CD44 and negatively related with CD24 and CD133 from analysis of GSE75034 and GSE7410 data sets (Figures S8A-C).

Moreover, immunohistochemistry analysis and statistical scores of the protein levels of cPLA₂α, E-cadherin, and vimentin in 99 CC patients with or without lymph node metastasis showed that cPLA₂α was overexpressed in cervical tumor tissues relative to its expression in normal cervical tissues adjacent to tumor (Figure 7D,E). Western blotting on proteins extracted from another four pairs of fresh-frozen tissues further verified that the cPLA₂α level in tumor tissues was considerably higher than that in normal tissues (Figure 7F).

Clinicopathological analysis revealed that cPLA₂α expression was associated with the preoperative squamous cell carcinoma antigen

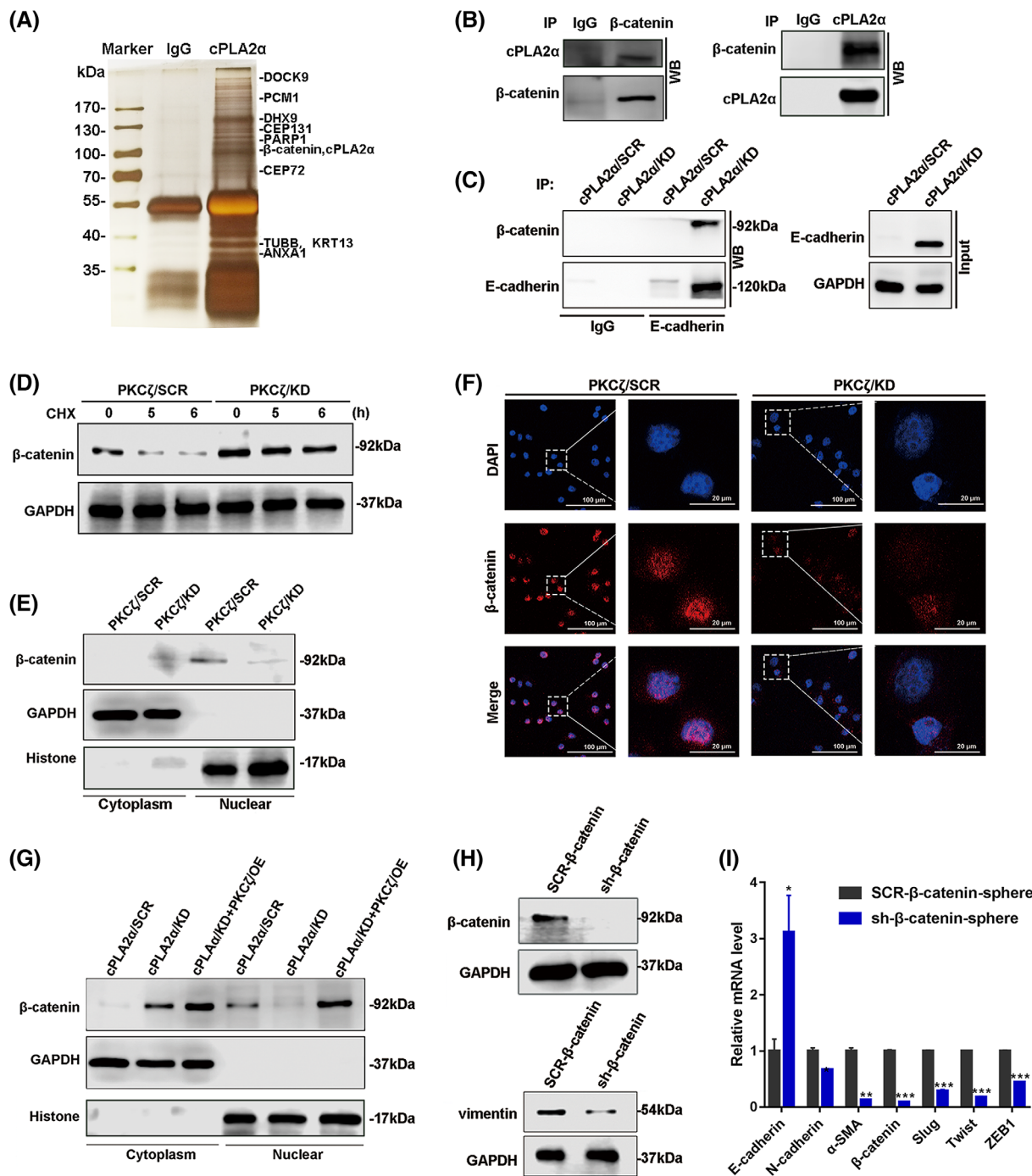


FIGURE 6 cPLA α regulates phosphorylation of PKC ζ , which further promotes β-catenin translocation into the nucleus to affect the stem cell phenotype. A, Whole-cell extracts from HeLa cells were incubated with protein-A magnetic beads coupled with cPLA α antibody. After full washing, the cPLA α -containing immune complexes were separated by 10% SDS-PAGE electrophoresis. The binding protein bands were visualized by silver staining, and the representative peptide fragments were shown and identified by mass spectrometry. B, Whole-cell lysates from HeLa cells were immunoprecipitated (IP) followed by Western blotting (WB) with antibodies against the indicated molecules. C, The lysates from cPLA α KD and SCR cells were used for co-immunoprecipitation assays with an anti-E-cadherin antibody followed by WB with an anti-β-catenin antibody. D, WB analysis of β-catenin expression in PKC ζ SCR and PKC ζ KD cells that treated with 100 μg/mL CHX at 0, 5, and 6 hours. E, The nuclear and cytoplasmic protein fractions were obtained to identify the corresponding β-catenin levels in cells with distinct expression levels of PKC ζ . F, PKC ζ KD and SCR cells were immunostained with antibodies against β-catenin. Representative images are shown. G, cPLA α KD cells were induced by the Tet-on inducible system to overexpress PKC ζ , and the cellular extracts were used to analyze the level of β-catenin in the nucleus and cytoplasm. H, HeLa cells were stably transfected with β-catenin shRNA, and WB was used to verify the levels of β-catenin and vimentin. I, The levels of EMT-related genes were determined by RT-PCR in the sh-β-catenin and SCR-β-catenin groups (*P < .05; **P < .01; ***P < .001). cPLA α , cytosolic phospholipase A2 α ; EMT, epithelial-mesenchymal transition

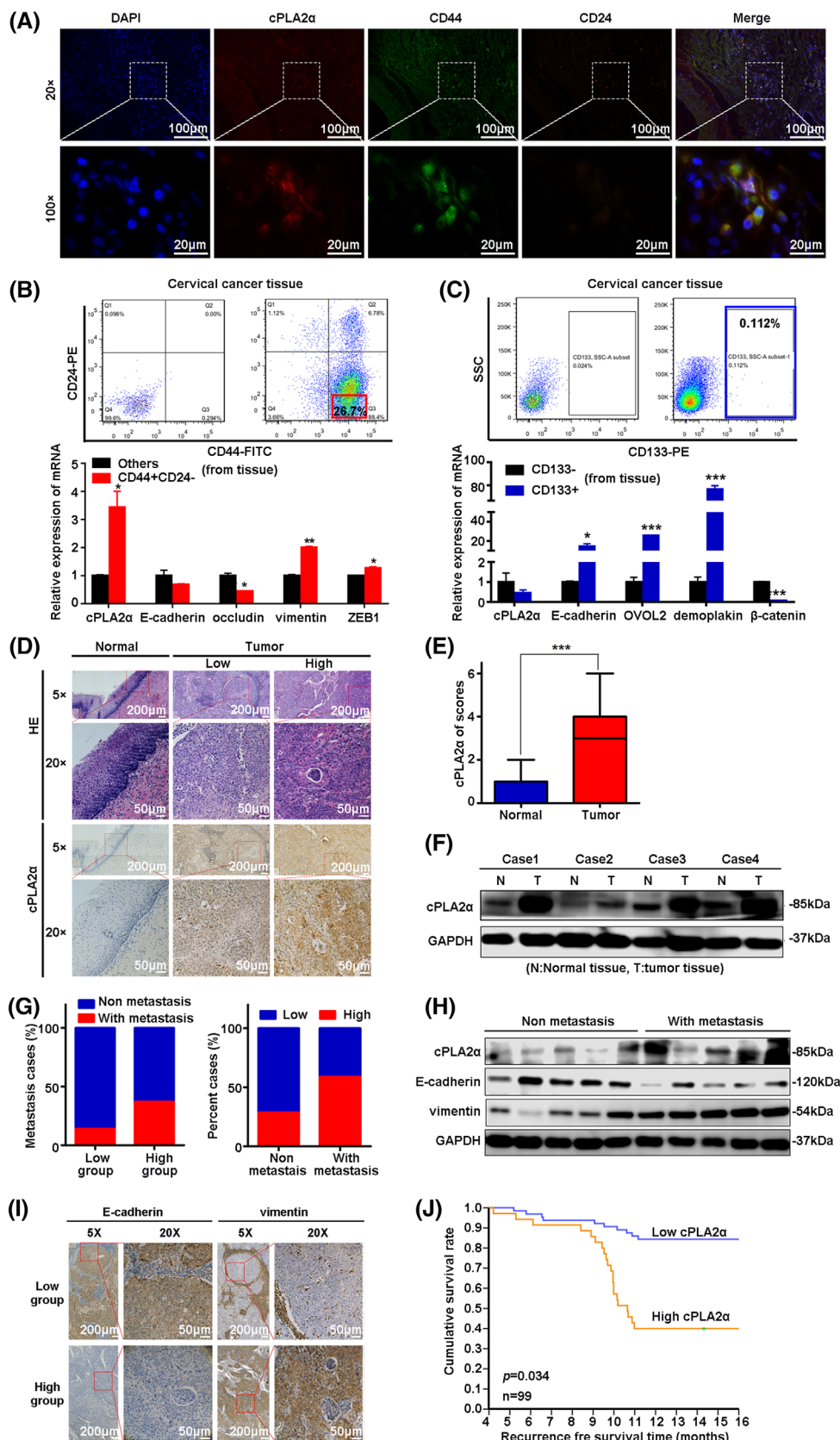


FIGURE 7 Elevated cPLA2 α expression is associated with cervical cancer metastasis and poor survival. A, Localization and staining of cPLA2 α (red), CD44 (green), CD24 (brown), and DAPI (blue) in clinical primary cervical cancer tissues as assessed by immunofluorescence assay. Scale bars = 100 and 20 μ m. B, C, Fresh cervical cancer tissues were sorted into two populations labeled CD44 $^+$ CD24 $^-$ and CD133 $^+$ by flow cytometry. Then, RNA was extracted and amplified with the smart-seq method to obtain cDNA for quantitative analysis of EMT or MET gene expression by RT-PCR. D, Representative photomicrographs of HE staining and immunostaining for cPLA2 α in normal tissue and tumor tissue with different intensities. Scale bars = 200 and 50 μ m. E, cPLA2 α score statistics between the normal and tumor groups. F, The cPLA2 α protein level was measured by Western blotting in four pairs of tumor and adjacent tissues. G, Immunohistochemical scores of cPLA2 α in 99 cervical cancer patients were classified as low and high, and the correlation of cPLA2 α expression with cervical cancer metastasis was analyzed. H, Western blot detection of cPLA2 α , E-cadherin, and vimentin in metastatic and nonmetastatic tumor tissues. I, Representative E-cadherin and vimentin staining in the cPLA2 α -low and cPLA2 α -high groups. Scale bars = 200 and 50 μ m. J, Kaplan-Meier analysis of RFS revealed that cPLA2 α overexpression was associated with poorer prognosis in a sample of 99 cervical cancer patients ($^*P < .05$; $^{**}P < .01$; $^{***}P < .001$). cPLA2 α , cytosolic phospholipase A2 α ; EMT, epithelial-mesenchymal transition; HE, hematoxylin and eosin; MET, mesenchymal-epithelial transition; RFS, recurrence free survival

level, tumor size, lymph node metastasis, and vascular tumor thrombus (Table S3), indicating that cPLA2 α expression was linked with aggressive carcinogenic behavior in CC. Notably, clinical investigation

revealed that 37.1% of cancer patients with high expression of cPLA2 α experienced metastasis, a higher percentage than seen in the group with low expression of cPLA2 α (14.1%) (Figure 7G). In addition,

patients with metastasis exhibited increased cPLA₂ α levels (Figure 7G,H). Patients with high expression of cPLA₂ α had a higher risk of metastasis.

EMT has been associated with cancer metastasis.^{36,37} Compared with nonmetastatic tumor tissues with lower cPLA₂ α expression, metastatic tissues with higher cPLA₂ α expression displayed decreased expression of E-cadherin and increased expression of vimentin (Figure 7H). Consistent with the immunohistochemical staining results, the high cPLA₂ α expression group exhibited stronger vimentin staining and lower E-cadherin expression than the low cPLA₂ α expression group (Figure 7I and Figure S8D). TCGA database analysis further confirmed the correlation between cPLA₂ α and EMT-related markers. cPLA₂ α expression was negatively correlated with the expression of epithelial marker E-cadherin (Figure S8E) and positively correlated with the expression of mesenchymal markers such as N-cadherin and β -catenin (Figures S8F,G).

Among the 99 patients with CC and adequate clinical follow-up, patients with either metastasis or higher expression of cPLA₂ α had poor RFS (Figure 7J and Figure S8H). Multivariate analysis revealed that the level of cPLA₂ α (HR = 2.618, 95% CI = 1.074-6.385, P = .034) and lymph node metastasis (HR = 3.233, 95% CI = 1.236-8.457, P = .017) were the independent risk factors associated with RFS in CC (Table S4).

Considering our abovementioned findings, we conclude that cPLA₂ α reversibly regulates the transformation of CCSCs from the quiescent epithelial-like to malignant mesenchymal-like states by regulating the phosphorylation of PKC ζ , which further inhibits β -catenin-E-cadherin interaction in membrane and promotes β -catenin translocation into the nucleus to affect the stem cell phenotype and metastasis in CC, as shown in Figure S9.

4 | DISCUSSION

The final step of cancer progression is metastasis, which causes >90% of cancer-related deaths. Although metastatic spread occurs late in cancer progression, some study results demonstrated that cancer cell dissemination occurs in a clinically latent stage before the manifestation of metastasis. Unfortunately, at least 80% of metastases are derived from early disseminated cancer cells.³⁸⁻⁴⁰ Understanding the initiation and progression of metastasis is pivotal to developing new clinical therapeutic strategies to treat and prevent cancer metastasis.

With the development of CSC theory, some studies hold that CSCs could serve as a crucial factor for tumor recurrence and metastasis. Lawson et al reported that metastases are initiated by CSCs that proliferate and differentiate to produce advanced metastasis.⁴¹ However, CSCs display heterogeneity, possess different cell characteristics and cell surface markers, and can self-renew and generate heterogeneous lineages of cancer cells. CSCs exist in distinct mesenchymal-like (EMT-like) and epithelial-like (non-EMT-like) states with different levels of cellular plasticity and invasive and proliferative potential in hepatocellular carcinoma and breast cancer.^{10,42} However, no evidence was found on the different phenotypes of CCSCs. Here, we

first screened two morphologically distinct CSCs populations classified by different expression levels of cPLA₂ α in CC. cPLA₂ α ^{high} identified the CD44⁺CD24⁻ CCSC phenotype with mesenchymal traits, and cPLA₂ α ^{low} identified the CD133⁺ CCSC phenotype with epithelial characteristics. Our studies may provide a unique marker (cPLA₂ α) to distinguish different CSCs phenotypes in CC.

Generally, cancer stem-like cells maintain a quiescent state characterized by cell cycle stagnation in G0/G1 and slow proliferation and tumorigenic ability.⁴³⁻⁴⁵ Once some pivotal genes are activated in the microenvironment, the quiescent CSCs will promote malignant potential, rejuvenate, and transfer to the invasive and metastatic subset.^{45,46} Here, we found that the epithelial CCSCs with low cPLA₂ α expression were quiescent with cell cycle arrest and slight tumorigenesis. cPLA₂ α triggered the transformation of CD133⁺ quiescent stem-like cells to progressive status (CD44⁺CD24⁻), which display high proliferation, invasion, adhesion, and spreading abilities that are consistent with recent reports.^{25,26} cPLA₂ α plays a critical role in tumorigenesis, and its deletion of cPLA₂ α inhibits mouse lung tumorigenesis.⁴⁷ We also reported that cPLA₂ α was required for the maintenance of the tumor initiation capacity of CCSCs in a gene dose-dependent manner.

Accumulating studies have highlighted a relationship between CSCs and the acquisition of an EMT state.^{7,48,49} These CSCs possess different gene signals and rapidly switch the transcriptional machinery to enter an EMT state or a non-EMT state when tumor conditions change or the invasive edge becomes the interior of the tumor.^{13,16} Previous studies have suggested that metastatic cancer cells utilize an EMT program to promote stemness and facilitate dissemination,^{7,22,50} whereas other studies suggested that EMT and CSCs are mutually exclusive.⁴¹ Our study proposes a model in which CCSCs exist in alternative epithelial-like and mesenchymal-like subsets that are reversibly regulated by the cPLA₂ α expression level and display distinct gene expression profiles and cell characteristics. Furthermore, CCSCs display reversible cellular plasticity with different cPLA₂ α expression levels, which enables them to transition between the mesenchymal-like and epithelial-like states, associated with quiescent cells activation. The plasticity of the different CSC states may play a fundamental role in tumor progression and treatment resistance. Thus, targeting CSC plasticity to eliminate these lethal cancer seeds may hold great potential value.

Our previous studies demonstrated that cPLA₂ α can mediate EMT through PI3k/Akt signaling in hepatocellular carcinoma and breast cancer cells.^{20,21} Using a phosphoantibody microarray-based proteomic approach, we found hyperphosphorylation of PI3k/Akt signaling components in cPLA₂ α -overexpressing cells. PKC ζ , an atypical protein kinase C, is a key component of PI3k/Akt signaling that can direct cell fate decisions to govern cancer cell state changes (a stem cell-like state vs a differentiation state).^{30,31} A very recent study demonstrated that PKC ζ is a critical regulator of colorectal cancer cell EMT and metastasis through modulating miR-200.⁵¹ Moreover, combined inactivation of PKC ζ and COX-2 induced MET in melanoma cells, which in turn inhibited migration and invasion.⁵² Machida et al reported that NANOG-AURKA-PKC ζ signaling is an important regulatory pathway for liver tumor-initiating cell events such as self-renewal and tumorigenesis.⁵³ Here, we observed the

positive regulation of PKC ζ by cPLA2 α in CCSCs, which is likely at least partially responsible for the cPLA2 α -mediated transition of CCSCs between the mesenchymal-like and epithelial-like states. Our data suggest that PKC ζ overexpression in cPLA2 α -knockdown CCSCs rescued mesenchymal-like CSC events, such as mesenchymal marker expression and high clonogenic capacity.

PKC ζ affects β -catenin stability, further affecting stem cell function.³³ The Wnt/ β -catenin pathway plays an important role in tumor cell EMT and stemness⁵⁴⁻⁵⁶; such report is consistent with our results from KEGG pathway analysis based on the differential genes between cPLA2 α KD and KD/SCR CSCs and from mass spectrometry analysis. Many β -catenin molecules bound to the cytomembrane with E-cadherin, and less nuclear translocation of β -catenin occurred when PKC ζ was knocked down regulated by cPLA2 α inhibition, leading to increased E-cadherin-mediated cell-to-cell adhesion and blockage of EMT and metastasis.

5 | CONCLUSION

In summary, our results suggest for the first time that CSCs can exist in alternative quiescent mesenchymal-like and invasive epithelial-like states in CC. cPLA2 α triggers the transformation of quiescent CD133 $^+$ CCSCs to CD44 $^+$ CD24 $^-$ mesenchymal-like CCSCs by reversibly regulating the phosphorylation of PKC ζ . This process further inhibits β -catenin-E-cadherin interaction in the membrane and promotes β -catenin translocation into the nucleus to affect the stem cell phenotype and metastasis in CC. Our results identify potentially important new targets for therapeutic interventions to inhibit the transformation of quiescent CCSCs and halt tumor recurrence and metastatic spread. Further analyses of the transition between the different CCSC states may accelerate the development of combination therapies.

ACKNOWLEDGMENTS

This work was supported by the grants from Key Project of Tianjin Natural Science Foundation (18JCZDJC35200), NSFC-FRQS program (81661128009), State Key Project on Infectious Diseases of China (2018ZX10723204), NSFC (31671421).

CONFLICT OF INTEREST

The authors declared no potential conflicts of interest.

AUTHOR CONTRIBUTIONS

Y.H., H.F.: conception and design, collection and/or assembly of data, data analysis and interpretation, financial support, administrative support, manuscript writing, final approval of manuscript; M.X.: collection and/or assembly of data, data analysis and interpretation, manuscript writing, final approval of manuscript; Lu Chen, L.Q., H.X., D.L.: provision of study material or patients, data analysis and interpretation; P.G., Liwei Chen, Y.L.: collection and/or assembly of data, administrative support; N.Z., H.G.: conception and design, financial support, administrative support, manuscript writing, final approval of manuscript.

DATA AVAILABILITY STATEMENT

The data used and/or analyzed during the current study are available from the corresponding author on reasonable request.

ORCID

Hua Guo  <https://orcid.org/0000-0002-3345-8005>

REFERENCES

- Allemani C, Matsuda T, Di Carlo V, et al. Global surveillance of trends in cancer survival 2000-14 (CONCORD-3): analysis of individual records for 37 513 025 patients diagnosed with one of 18 cancers from 322 population-based registries in 71 countries. *Lancet*. 2018; 391:1023-1075.
- Siegel RL, Miller KD, Jemal A. Cancer statistics, 2018. *CA Cancer J Clin*. 2018;68:7-30.
- Tyagi A, Vishnoi K, Mahata S, et al. Cervical cancer stem cells selectively overexpress HPV Oncoprotein E6 that controls stemness and self-renewal through upregulation of HES1. *Clin Cancer Res*. 2016;22: 4170-4184.
- Medema JP. Cancer stem cells: the challenges ahead. *Nat Cell Biol*. 2013;15:338-344.
- Tejero R, Huang Y, Katsiyi I, et al. Gene signatures of quiescent glioblastoma cells reveal mesenchymal shift and interactions with niche microenvironment. *EBioMedicine*. 2019;42:252-269.
- Ho MM, Ng AV, Lam S, Hung JY. Side population in human lung cancer cell lines and tumors is enriched with stem-like cancer cells. *Cancer Res*. 2007;67:4827-4833.
- Mani SA, Guo W, Liao MJ, et al. The epithelial-mesenchymal transition generates cells with properties of stem cells. *Cell*. 2008;133: 704-715.
- Mima K, Okabe H, Ishimoto T, et al. CD44s regulates the TGF-beta-mediated mesenchymal phenotype and is associated with poor prognosis in patients with hepatocellular carcinoma. *Cancer Res*. 2012;72: 3414-3423.
- Nieto MA, Huang RY, Jackson RA, et al. Emt: 2016. *Cell*. 2016;166: 21-45.
- Pastushenko I, Brisebarre A, Sifrim A, et al. Identification of the tumour transition states occurring during EMT. *Nature*. 2018;556: 463-468.
- Ye X, Weinberg RA. Epithelial-mesenchymal plasticity: a central regulator of cancer progression. *Trends Cell Biol*. 2015;25:675-686.
- Biddle A, Liang X, Gammon L, et al. Cancer stem cells in squamous cell carcinoma switch between two distinct phenotypes that are preferentially migratory or proliferative. *Cancer Res*. 2011;71:5317-5326.
- Liu S, Cong Y, Wang D, et al. Breast cancer stem cells transition between epithelial and mesenchymal states reflective of their normal counterparts. *Stem Cell Rep*. 2014;2:78-91.
- Lopez J, Poitevin A, Mendoza-Martinez V, et al. Cancer-initiating cells derived from established cervical cell lines exhibit stem-cell markers and increased radioresistance. *BMC Cancer*. 2012;12:48.
- Yu VY, Nguyen D, Pajonk F, et al. Incorporating cancer stem cells in radiation therapy treatment response modeling and the implication in glioblastoma multiforme treatment resistance. *Int J Radiat Oncol Biol Phys*. 2015;91:866-875.
- Zheng H, Pomyen Y, Hernandez MO, et al. Single-cell analysis reveals cancer stem cell heterogeneity in hepatocellular carcinoma. *Hepatology*. 2018;68:127-140.
- Tu K, Dou C, Zheng X, et al. Fibulin-5 inhibits hepatocellular carcinoma cell migration and invasion by down-regulating matrix metalloproteinase-7 expression. *BMC Cancer*. 2014;14:938.
- Linkous A, Geng L, Lyshchik A, Hallahan DE, Yazlovitskaya EM. Cytosolic phospholipase A2: targeting cancer through the tumor vasculature. *Clin Cancer Res*. 2009;15:1635-1644.

19. Gandhi UH, Kaushal N, Hegde S, et al. Selenium suppresses leukemia through the action of endogenous eicosanoids. *Cancer Res.* 2014;74: 3890-3901.
20. Chen L, Fu H, Luo Y, et al. cPLA2 alpha mediates TGF-beta-induced epithelial-mesenchymal transition in breast cancer through PI3k/Akt signaling. *Cell Death Dis.* 2017;8:e2728.
21. Fu H, He Y, Qi L, et al. cPLA2 alpha activates PI3K/AKT and inhibits Smad2/3 during epithelial-mesenchymal transition of hepatocellular carcinoma cells. *Cancer Lett.* 2017;403:260-270.
22. Wellner U, Schubert J, Burk UC, et al. The EMT-activator ZEB1 promotes tumorigenicity by repressing stemness-inhibiting microRNAs. *Nat Cell Biol.* 2009;11:1487-1495.
23. Oikawa T, Wauthier E, Dinh TA, et al. Model of fibrolamellar hepatocellular carcinomas reveals striking enrichment in cancer stem cells. *Nat Commun.* 2015;6:8070.
24. Li S, Yang J. Ovol proteins: guardians against EMT during epithelial differentiation. *Dev Cell.* 2014;29:1-2.
25. Yano S, Tazawa H, Hashimoto Y, et al. A genetically engineered oncolytic adenovirus decoys and lethally traps quiescent cancer stem-like cells in S/G2/M phases. *Clin Cancer Res.* 2013;19:6495-6505.
26. Weng MY, Li L, Feng SY, Hong SJ. Expression of Bmi-1, P16, and CD44v6 in uterine cervical carcinoma and its clinical significance. *Cancer Biol Med.* 2012;9:48-53.
27. Gomez-Martinez M, Schmitz D, Hergovich A. Generation of stable human cell lines with tetracycline-inducible (Tet-on) shRNA or cDNA expression. *J Vis Exp.* 2013;73:e50171.
28. Dubrovska A, Kim S, Salamone RJ, et al. The role of PTEN/Akt/PI3K signaling in the maintenance and viability of prostate cancer stem-like cell populations. *Proc Natl Acad Sci U S A.* 2009;106:268-273.
29. Hardt O, Wild S, Oerlecke I, et al. Highly sensitive profiling of CD44+/CD24- breast cancer stem cells by combining global mRNA amplification and next generation sequencing: evidence for a hyperactive PI3K pathway. *Cancer Lett.* 2012;325:165-174.
30. Wu MJ, Chen YS, Kim MR, et al. Epithelial-mesenchymal transition directs stem cell polarity via regulation of mitofusin. *Cell Metab.* 2019; 29:993-1002.e1006.
31. Miura T, Kume M, Kawamura T, Yamamoto K, Hamakubo T, Nishihara S. O-GlcNAc on PKCzeta inhibits the FGF4-PKCzeta-MEK-ERK1/2 pathway via inhibition of PKCzeta phosphorylation in mouse embryonic stem cells. *Stem Cell Rep.* 2018;10:272-286.
32. Burban A, Sharnek A, Hue R, et al. Penicillinase-resistant antibiotics induce non-immune-mediated cholestasis through HSP27 activation associated with PKC/P38 and PI3K/AKT signaling pathways. *Sci Rep.* 2017;7:1815.
33. Llado V, Nakanishi Y, Duran A, et al. Repression of intestinal stem cell function and tumorigenesis through direct phosphorylation of beta-catenin and yap by PKCzeta. *Cell Rep.* 2015;10:740-754.
34. Shang S, Hua F, Hu ZW. The regulation of beta-catenin activity and function in cancer: therapeutic opportunities. *Oncotarget.* 2017;8: 33972-33989.
35. Onder TT, Gupta PB, Mani SA, et al. Loss of E-cadherin promotes metastasis via multiple downstream transcriptional pathways. *Cancer Res.* 2008;68:3645-3654.
36. Aiello NM, Brabletz T, Kang Y, Nieto MA, Weinberg RA, Stanger BZ. Upholding a role for EMT in pancreatic cancer metastasis. *Nature.* 2017;547:E7-E8.
37. Ye X, Brabletz T, Kang Y, et al. Upholding a role for EMT in breast cancer metastasis. *Nature.* 2017;547:E1-E3.
38. Harper KL, Sosa MS, Entenberg D, et al. Mechanism of early dissemination and metastasis in Her2(+) mammary cancer. *Nature.* 2016;540: 588-592.
39. Hosseini H, Obradovic MM, Hoffmann M, et al. Early dissemination seeds metastasis in breast cancer. *Nature.* 2016;540:552-558.
40. Husemann Y, Geigl JB, Schubert F, et al. Systemic spread is an early step in breast cancer. *Cancer Cell.* 2008;13:58-68.
41. Lawson DA, Bhakta NR, Kessenbrock K, et al. Single-cell analysis reveals a stem-cell program in human metastatic breast cancer cells. *Nature.* 2015;526:131-135.
42. Malfettone A, Soukupova J, Bertran E, et al. Transforming growth factor-beta-induced plasticity causes a migratory stemness phenotype in hepatocellular carcinoma. *Cancer Lett.* 2017;392:39-50.
43. Ito K, Bernardi R, Morotti A, et al. PML targeting eradicates quiescent leukaemia-initiating cells. *Nature.* 2008;453:1072-1078.
44. Saito Y, Uchida N, Tanaka S, et al. Induction of cell cycle entry eliminates human leukemia stem cells in a mouse model of AML. *Nat Biotechnol.* 2010;28:275-280.
45. Lagadinou ED, Sach A, Callahan K, et al. BCL-2 inhibition targets oxidative phosphorylation and selectively eradicates quiescent human leukemia stem cells. *Cell Stem Cell.* 2013;12:329-341.
46. Jiang YX, Yang SW, Li PA, et al. The promotion of the transformation of quiescent gastric cancer stem cells by IL-17 and the underlying mechanisms. *Oncogene.* 2017;36:1256-1264.
47. Meyer AM, Dwyer-Nield LD, Hurteau GJ, et al. Decreased lung tumorigenesis in mice genetically deficient in cytosolic phospholipase A2. *Carcinogenesis.* 2004;25:1517-1524.
48. Latil M, Nassar D, Beck B, et al. Cell-type-specific chromatin states differentially prime squamous cell carcinoma tumor-initiating cells for epithelial to mesenchymal transition. *Cell Stem Cell.* 2017;20:191-204.e195.
49. Celia-Terrassa T, Meca-Cortes O, Mateo F, et al. Epithelial-mesenchymal transition can suppress major attributes of human epithelial tumor-initiating cells. *J Clin Invest.* 2012;122:1849-1868.
50. Rhim AD, Mirek ET, Aiello NM, et al. EMT and dissemination precede pancreatic tumor formation. *Cell.* 2012;148:349-361.
51. Shelton PM, Duran A, Nakanishi Y, et al. The secretion of miR-200s by a PKCzeta/ADAR2 signaling axis promotes liver metastasis in colorectal cancer. *Cell Rep.* 2018;23:1178-1191.
52. Zhou P, Qin J, Li Y, et al. Combination therapy of PKCzeta and COX-2 inhibitors synergistically suppress melanoma metastasis. *J Exp Clin Cancer Res.* 2017;36:115.
53. Siddique HR, Feldman DE, Chen CL, Punj V, Tokumitsu H, Machida K. NUMB phosphorylation destabilizes p53 and promotes self-renewal of tumor-initiating cells by a NANOG-dependent mechanism in liver cancer. *Hepatology.* 2015;62:1466-1479.
54. Zhang J, Cai H, Sun L, et al. LGR5, a novel functional glioma stem cell marker, promotes EMT by activating the Wnt/beta-catenin pathway and predicts poor survival of glioma patients. *J Exp Clin Cancer Res.* 2018;37:225.
55. Liang Z, Lu L, Mao J, Li X, Qian H, Xu W. Curcumin reversed chronic tobacco smoke exposure induced urocystic EMT and acquisition of cancer stem cells properties via Wnt/beta-catenin. *Cell Death Dis.* 2017;8:e3066.
56. He J, Zhou M, Chen X, et al. Inhibition of SALL4 reduces tumorigenicity involving epithelial-mesenchymal transition via Wnt/beta-catenin pathway in esophageal squamous cell carcinoma. *J Exp Clin Cancer Res.* 2016;35:98.

SUPPORTING INFORMATION

Additional supporting information may be found online in the Supporting Information section at the end of this article.

How to cite this article: He Y, Xiao M, Fu H, et al. cPLA₂ α reversibly regulates different subsets of cancer stem cells transformation in cervical cancer. *Stem Cells.* 2020;38: 487-503. <https://doi.org/10.1002/stem.3157>